Journal of Mammalian Evolution
https://doi.org/10.1007/s10914-018-9455-8

ORIGINAL PAPER

Feeding Biomechanics Influences Craniofacial Morphology at the Subspecies Scale among Australian Pademelons (Macropodidae: *Thylogale*)

D. Rex Mitchell[1] · Emma Sherratt[2] · Gabriele Sansalone[1] · Justin A. Ledogar[1,3] · Richard J. Flavel[4] · Stephen Wroe[1]

Abstract
Interspecific variation in the craniofacial morphology of kangaroos and wallabies is associated with diet and feeding behaviors. Yet, to how fine a taxonomic scale this relationship might exist is unknown. Using a combination of established morphometric analyses and novel finite element approaches, we test the limits of these associations by examining three closely-related pademelon taxa: the red-necked pademelon (*Thylogale thetis*), and two subspecies of the red-legged pademelon (*Thylogale stigmatica stigmatica* and *Thylogale stigmatica wilcoxi*). All three taxa have distinct proportions of graze (grasses) and browse (leaves, stems, and branches of trees and shrubs) in their diets. We identified clear morphological differences in the crania between all three taxa and significant influences of geography and climate on cranial shape. We found significant differences in shape and strain magnitudes along the muzzle and cheek bones of each group that are consistent with the properties of their respective diets. These results suggest that feeding ecology influences craniofacial morphology down to the subspecies scale for at least some kangaroos and wallabies, which mirrors what is known at the macroevolutionary level for these species. This lends further weight to the predictive value of cranial morphology in determining feeding ecology among the Macropodiformes and may be of use in inferring feeding ecology of less accessible species for conservation and management.

Keywords Herbivory · Finite element analysis · Geometric morphometrics · Marsupial · Cranium · Evolution

Introduction

Herbivorous mammals display morphological and physiological attributes that relate to feeding ecology (Shipley 1999; Clauss et al. 2008). Cranial morphometric analyses of the Macropodiformes (kangaroos, wallabies, bettongs, potoroos, and the musky rat kangaroo) have identified differences in cranial shape to within genera that are associated with feeding (Milne and O'Higgins 2002; Mitchell et al. 2018). Mitchell et al. (2018) conducted a study spanning sixteen species, representing three families, and found that muzzle morphology across this taxon is closely associated with feeding biomechanics. Relatively shorter muzzles, in particular, were associated with increased mechanical efficiency (output force/input force) and decreased bone deformation during hard biting on resistant vegetation. However, to how fine a taxonomic scale that feeding ecology can predict craniofacial morphology among macropodiforms is unknown. In this study, we test the limits of these findings by examining the influence of diet across three closely related pademelon taxa.

The red-legged pademelon, *Thylogale stigmatica*, is a small macropod (~6.8 kg), with a species complex that has a disjunct distribution from New Guinea to southeastern New South Wales (NSW), Australia (Fig. 1): *T. s. oriomo* is found in New Guinea, *T. s. coxenii* is from far north Queensland

Electronic supplementary material The online version of this article (https://doi.org/10.1007/s10914-018-9455-8) contains supplementary material, which is available to authorized users.

✉ D. Rex Mitchell
drexmitch311@gmail.com

[1] Zoology Division, School of Environmental and Rural Science, University of New England, Armidale, NSW 2351, Australia

[2] Department of Ecology and Evolutionary Biology, School of Biological Sciences, University of Adelaide, Adelaide, SA 5005, Australia

[3] Department of Evolutionary Anthropology, Duke University, Durham, NC 27708, USA

[4] Agronomy and Soil Science, School of Environmental and Rural Science, University of New England, Armidale, NSW 2351, Australia

Published online: 14 November 2018

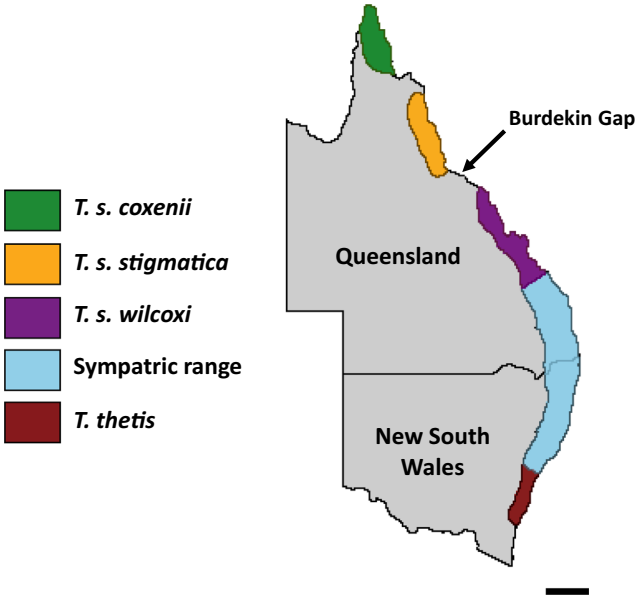

Fig. 1 Distribution of mainland Australian *Thylogale* spp. Sympatric range of *Thylogale s. wilcoxi* and *Thylogale thetis* is marked in blue. Scale bar = 500 km. (modified from ALA, 2016). *Thylogale s. coxenii* is not included in this study but shown for completeness

(QLD), *T. s. stigmatica* is found in the fragmented tropical rainforests from Annan National Park, QLD to Mackay, QLD, and *T. s. wilcoxi* inhabits the moist sclerophyll forests from Rockhampton, QLD to Wyong, NSW (Vernes 1995; Eldridge et al. 2011). The distributions of *T. s. stigmatica* and *T. s. wilcoxi* are separated by a dry habitat barrier, the Burdekin Gap (Macqueen et al. 2012). A closely related species, the red-necked pademelon (*Thylogale thetis*), is also found along the east coast of Australia, from Bundaberg, QLD to Jervis Bay, NSW and is sympatric with *T. s. wilcoxi* for the majority of its northern range (Vernes 1995) (Fig. 1).

The behavioral ecologies exhibited by *T. stigmatica* subspecies in eastern Australia are influenced by the presence of *T. thetis,* which frequently inhabits the ecotone between forest and pasture (Johnson 1977). *Thylogale s. stigmatica* displays comparable behavior to *T. thetis* in northern Queensland; sometimes reaching high densities and using forest/pasture ecotone for grazing (Jarman et al. 1987; Vernes 1995). In contrast, *T. s. wilcoxi,* occurs sympatrically with *T. thetis* across most of its range at low densities, remaining almost exclusively within the forest (Johnson 1980; Johnson and Vernes 2008). Hypotheses for the apparent exclusion of *T. s. wilcoxi* from the forest/pasture ecotone include direct aggression or prior grazing by the larger *T. thetis*, and the greater risk of predation on the smaller *T. s. wilcoxi* in pastures (Vernes 1995; Wahungu et al. 1999). The differences in behavioral ecology seen between these *T. stigmatica* subspecies have resulted in different diets. The diet of *T. s. stigmatica* comprises up to 51% monocot grasses (Vernes 1995), similar to that of *T. thetis*, which consumes up to 65% monocot grasses. However, *T. s. wilcoxi* feeds almost exclusively on dicot browse (Jarman 1984; Jarman and Phillips 1989) (Table 1). Diets of the two remaining subspecies; *T. s. oriomo* and *T. s. coxenii* have yet to be studied.

Given the apparent geographical and ecological differences outlined above, the two eastern Australian subspecies of *T. stigmatica* offer an ideal opportunity to examine the processes driving intraspecific variation in cranial morphology in macropods. The observed differences in diet found between *T. s. stigmatica* and *T. s. wilcoxi* may permit the identification of fine-scale adaptations to masticatory morphology required for obtaining and processing different vegetation types. Furthermore, *T. thetis* provides an opportunity to identify grazing attributes. Here, we use a combined geometric morphometrics and finite element analysis (FEA) approach to examine shape and biomechanical performance among the crania of these three pademelon taxa. Despite *T. stigmatica* being a mixed feeder with a relatively average macropod cranial morphology (see Mitchell et al. 2018), we hypothesized that the shape of the crania in the browsing *T. s. wilcoxi* would exhibit features adapted for obtaining and processing more resistant vegetation, such as a shorter, more robust muzzle and a zygomatic arch reflecting greater muscle development for hard biting (Warburton 2009; Mitchell et al. 2018). Further, we hypothesized that the crania of *T. s. stigmatica* would be more similar in morphology to crania of the ecologically similar *T. thetis*, despite climatic and geographical differences.

Methods

Geometric Morphometrics

We sampled specimens of *T. s. stigmatica*, *T. s. wilcoxi*, and *T. thetis*. *Thylogale. s. oriomo* and *T. s. coxenii* were not included because no dietary information exists for these subspecies. Only specimens with locality data were chosen; sampled from the Australian Museum; the Queensland Museum; and the Natural History Museum of the University of New England. The dataset included 12 *T. s. stigmatica*, 21; *T. s. wilcoxi*; and 19 *T. thetis* crania. Only adults were sampled

Table 1 Summary of dietary variation in *Thylogale* spp. of east Australia (from Jarman and Phillips 1989; Vernes 1995)

Species	monocots	dicots	ferns	fungi	unidentified
T. thetis	66%	32%	1%	1%	0%
T. s. stigmatica	51%	34%	10%	0%	5%
T. s. wilcoxi	0%	98%	1%	1%	0%

(i.e., M4 erupted) (Janis 1990). Their origins spanned the east coast from the Kuranda Range, QLD, to Wyong, NSW.

The 32 landmarks sampled from each specimen follow those of Mitchell et al. (2018) (see supplementary Fig. S1 and Table S1) and were digitized on the crania using a G2X Microscribe (Immersion Corporation, San Jose, CA) by one researcher. To account for measurement error, a subset of specimens was digitized three times. Mean Procrustes distances between specimens and between the three replicates were calculated. The proportion of variation found between specimens was calculated as a percentage of the combined variation contributed from between the three replicates and between the specimens (Zelditch et al. 2004). The measurement error was considered negligible if it contributed 5% or less of this variation.

Landmark data were analyzed using the *geomorph* package (v. 3.0.2) (Adams et al. 2016) in R v.3.2.5 (R Development Core Team 2016). These data were subjected to a generalized Procrustes superimposition to remove non-shape variation (Rohlf and Slice 1990). Object symmetry of paired landmarks was accounted for during superimposition (Klingenberg et al. 2002), using the geomorph function 'bilat.symmetry', and the symmetric component of shape was extracted and used as shape variables in all further analyses.

The influences of allometry and taxonomy on cranial shape were examined together by performing a Procrustes ANOVA, using the 'procD.lm' function with the formula shape ~ size*taxon, where shape is the Procrustes coordinates, size is the $\log_{10}$-transfomed centroid size, and taxon represents the three *Thylogale* taxa. We then compared the log10-transformed centroid size values between taxa to identify potential group differences in size via permuted ANOVA.

To test for the influence of geography and climate on cranial shape, we performed a variation partitioning analysis (VARPART, Legendre et al. 2012; Legendre and Legendre 2012) using the 'varpart' function in *vegan* R package v. 2.4–2 (Oksanen et al. 2013). This technique is used when two or more complementary sets of hypotheses are involved in explaining the variation of a response variable (Legendre 2008; Piras et al. 2010**;** Sansalone et al. 2015a, b). The latitude and longitude coordinates of each locality were transformed using the principal coordinates of neighbor matrices method (PCNM, Borcard and Legendre 2002; Borcard et al. 2004). We then tested the significance of the model performing a redundancy analysis (RDA). Bioclimate values for each specimen were extracted from data obtained from WORLDCLIM (v. 1.4) (the list of climate variables can be found at www.worldclim.org/bioclim). Considering the pairwise correlation between the predictors, we computed the variation inflation factors using a stepwise procedure. We then sub-selected the bioclimatic variables according to a threshold value of 10 (Carotenuto et al. 2016) and included six predictors: Mean Diurnal Range (BIO2), Isothermality (BIO3), Mean Temperature of Warmest Quarter (BIO10), Precipitation of Driest Month (BIO14), Precipitation of Warmest Quarter (BIO18), and Precipitation of Coldest Quarter (BIO19).

Principal component analysis (PCA) of the coordinate data was used to examine shape variation between the three taxa. To visualize the shape variation associated with the main PC axes, we used a 3D thin-plate spline warping approach (e.g., Klingenberg 2013; Sherratt et al. 2014) on a surface mesh (triangular isosurface) of the morphologically most-average specimen (*T. s. wilcoxi* UNE, NR0883).

Finite Element Analysis

Due to the time-consuming nature of generating finite element models (FEMs) (Grosse et al. 2007; Parr et al. 2012), intraspecific variation has rarely been addressed in previous FEA studies, with a single specimen typically being used to represent an entire species. A small number of studies have attempted to examine intraspecific variation in FEA (Kupczik et al. 2009; Oldfield et al. 2011; Fortuny et al. 2015; Smith et al. 2015a). However, in each case, few models were tested and there was no statistical support available for interpretations. With more powerful computers and improved software, we are now able to address this issue by including replicates for each taxon of interest. This provides the potential for statistical support and more concrete evidence for variations in biomechanical performance. This approach has recently been applied to test for significant differences at fixed landmarks between species (Ledogar et al. 2016). However, examination of strain along curves, represented by equally spaced semilandmarks might better show distributions in deformation along important structures and has not yet been attempted using replicates. Therefore, we include replicate FEMs for each taxon in this study to better identify differences in performance, along curves with relevance to feeding, between closely related species.

In order to best represent the morphological diversity, six specimens from each group were selected based upon their good condition for modelling (i.e., no breakages) and morphology that best approximated the extremes of the first three principal components (Pierce et al. 2008, 2009; Smith et al. 2015a, 2015b). Twelve specimens were scanned using a GE-Phoenix V|tome|xs 240 micro CT scanner (manufactured 2010, GE Sensing & Inspection Technologies GmbH, Niels-Bohr-Straße 7, 31,515 Wunstorf, Germany) located at the University of New England, Armidale, NSW Australia. The samples were mounted on the rotating stage and imaged using the predetermined optimal X-ray tube settings (160 kV, 120 μA, 200 ms integration time per projection, focal spot 4 μm diameter) with an isotropic voxel side length of 125 μm. The remaining six specimens were scanned at the University of New South Wales, on an Inveon microCT

(Siemens, Victoria) at up to 300 ms exposure with voxel lengths ranging from 600 to 1000 μm.

Protocols of FEM assembly follow Mitchell et al. (2018). Each model was created in Mimics (v.19) and 3-matic (v.19). Models comprised approximately 1.7 million tetrahedral elements and were assigned homogeneous and isotropic material properties. Material properties representing an average for mammalian bone were used (Young's modulus: E = 20 GPa; Poisson's ratio: v = 0.3).

Seven masticatory muscle divisions of macropods (see Warburton 2009) were defined on each cranium (Fig. S2). Muscle cross-sectional areas were obtained from the dissection of a red-necked wallaby (*Macropus rufogriseus*) roadkill specimen (see Mitchell et al. 2018), and muscle forces were scaled for each model using cranial volume to the two-thirds power (Strait et al. 2010) (Table S2). These forces were applied to plate elements representing each muscle's origin and directed to their respective insertion sites on the mandible using Boneload (Grosse et al. 2007). Models were restrained to simulate a bilateral incisor bite (I1), and unilateral premolar (P3) and molar (M3) bites. For a bilateral bite, a node was selected in each temporomandibular joint (TMJ) and restrained against translation for all axes, while a node was selected at each I1 incisor and restrained against the dorso-ventral axis only. For unilateral bites, the working side TMJ was only restrained in the dorso-ventral and anteroposterior axes, while a node at each tooth of interest was restrained only in the dorso-ventral axis (Fig. S3).

The FEMs were solved for strain using a linear static analysis in Strand 7 v. 2.4.4. We used von Mises (VM) strain to visually represent the results of our models, as the deformation and failure of bone is considered to follow a strain-controlled, ductile pattern (Nalla et al. 2003). Strain magnitudes were obtained along six curves of the cranium that have been observed to undergo deformation during feeding behaviors (see Sharp 2015; Mitchell et al. 2018) (Fig. 2); the dorsal muzzle (DM), the ventral orbit ridge (VOR), the dorsal (DZA) and ventral (VZA) zygomatic arch, the anterior ascending ridge of the masseteric process (AMP), and the proximal aspect of the diastema (D) (Fig. 2). Strain magnitudes were extracted using code that averages strain from the elements associated with nodes closest to respective semilandmarks. The strain magnitudes identified here represent relative, rather than absolute predictions of bone deformation. These do not reflect actual in vivo strain, but rather compare the performance of cranial shape and structure under equivalent muscle loads (Rayfield 2007).

Each curve was analyzed individually for each load case. To account for non-independence between semilandmarks, permutational multivariate analyses of variance (perMANOVAs) were carried out for strain magnitudes along each curve (1000 permutations). Post-hoc strain distributions were plotted to visualize strain distributions.

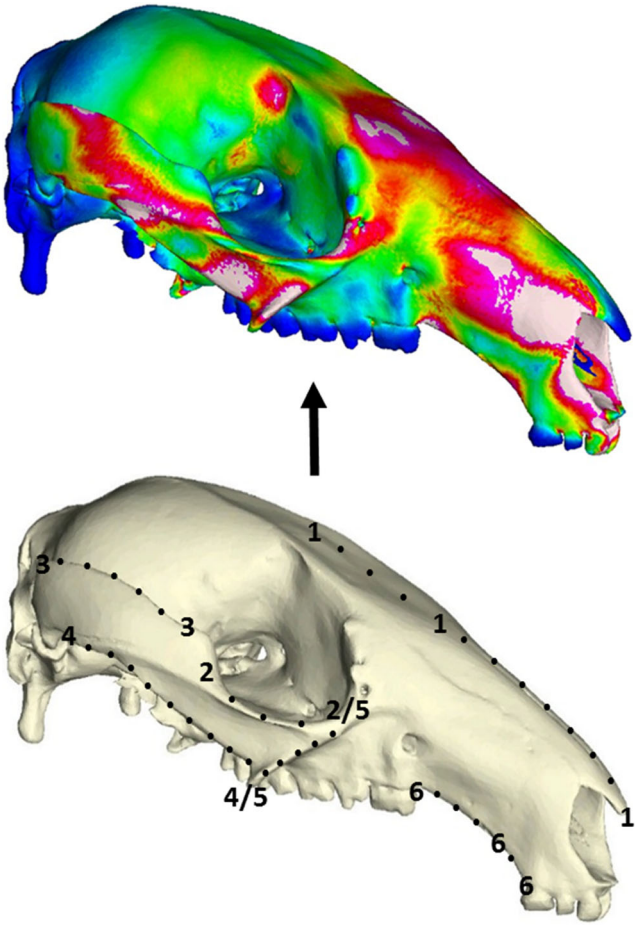

Fig. 2 Strain data is sampled from finite element models at equidistant semilandmarks along each curve for each bite simulation. Numbers indicate fixed landmarks on the curve. 1 = dorsal muzzle, 2 = ventral orbit ridge, 3 = dorsal zygomatic arch, 4 = ventral zygomatic arch, 5 = anterior masseteric process, 6 = lateral diastema. Shared fixed landmarks denoted by '/'

Tests conducted using the muzzle semilandmarks were carried out without the specimen that represented the maximum of PC3 for *T. s. wilcoxi*, as the muzzle of this specimen displayed unforeseen signs of damage in the results and returned strain magnitudes at least quadruple those of all other 17 specimens. Although this would only lend support to our predictions, it unfortunately had to be removed as an outlier for these semilandmarks, as it severely affected the group strain confidence intervals for *T. s. wilcoxi*.

Data Availability

The datasets generated during and/or analyzed during the current study, including specimen details, shape data, and strain data are available from the University of New England data repository, at RUNE (Research UNE; https://rune.une.edu.au/web/index.jsp). For access to image stacks or finite element models, please contact the author.

Results

The measurement error analysis revealed that 4.92% of the total variation was due to digitization error and therefore not a significant contribution to shape variation. There was a significant influence of allometry on cranial shape ($P = 0.001$); however, this only represented a small amount of variation ($R^2 = 0.055$). Taxonomy also significantly influenced shape, contributing greater variance than size ($R^2 = 0.265$, $F_{(2,46)} = 9.31$, $P = 0.001$); however, there was no interaction between allometry and taxonomy ($P = 0.059$), indicating that there was no difference in the allometric variation between taxa. Furthermore, centroid size was not significantly different between groups ($F = 0.556$, $P = 0.571$) (Fig. S4).

Variation Partitioning Analysis

The results of the variation partitioning analysis are summarized in Table 2 and the model is schematically represented in Fig. 3. Of the six independent climate variables, two (BIO2 and BIO3) had a significant influence on the shape data and were excluded from the variation partitioning model: mean diurnal range (MDR), representing mean of monthly (max. Temp. – min. Temp.) and isothermality (ISO) (mean diurnal range/annual temp. range). When testing the entire sample, both MDR and ISO showed a significant influence on cranial shape ($F_{(1,45)} = 2.15$, $R^2 = 0.041$, $P = 0.027$ and $F_{(1, 45)} = 3.11$, $R^2 = 0.058$, $P = 0.001$, respectively). This was also true for both subspecies alone ($F_{(1,26)} = 2.80$, $R^2 = 0.081$, $P < 0.001$ and $F_{(1,33)} = 1.64$, $R^2 = 0.047$, $P = 0.0323$).

Table 2 Variation partitioning analysis (VARPART) results of the effect of climate and geography on cranial shape. See Fig. 3 for schematic model. Bold values indicate significance ($P < 0.05$)

Cranial shape	df	R^2	R^2 (adj.)	*p*
Entire sample				
Full model	4	0.128	0.054	**0.008**
Individual fractions				
Pure geography	2	0.031	0.012	0.705
Pure climate	2	0.035	0.021	0.549
Fractions				
Entire geography	2	0.093	0.056	**0.002**
Entire climate	2	0.097	0.061	**0.001**
Subspecies only				
Full model	5	0.257	0.121	**0.001**
Individual fractions				
Pure geography	3	0.131	0.051	**0.006**
Pure climate	3	0.105	0.025	0.071
Fractions				
Entire geography	3	0.183	0.099	**0.001**
Entire climate	2	0.128	0.069	**0.001**

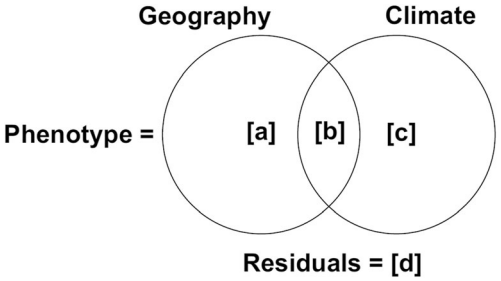

Fig. 3 Schematic representation of the VARPART analysis. The sums of a + b and b + c represent the entire fractions of geography and climate, respectively; a and c represent the pure fractions (see Table 3)

The VARPART models show a significant effect of climate and geography on cranial shape. However, geography is only significant when excluding *T. thetis* from the sample. When comparing only the subspecies, geography alone is significant (adj. $R^2 = 0.051$, $P = 0.006$); however, climate only contributes a significant amount of variation to cranial shape when considering the entire fraction (adj. $R^2 = 0.069$, $P = 0.001$) (see Table 2).

ANOVAs and Principal Component Analyses

The first PC axis (PC1) accounted for 25.4% of the total variance (Fig. 4), explained interspecific variation, and described four dominant shifts in cranial morphology. At the negative extreme of PC1, represented by *T. stigmatica*, the naso-frontal suture meets the midline in a more anterior location; the masseteric process is reduced and located more posteriorly on the zygomatic arch; the dorsal edge of the zygomatic arch is located more anteroventrally, resulting in a relatively shallow zygoma; and the dorsal orbit margin is located more anteriorly and laterally, widening the frontal plate between the orbits. The positive extreme of PC1 is dominated by *T. thetis*, and corresponds to the naso-frontal suture reaching the midline at a more posterior location; the masseteric process being more pronounced and flexed anteriorly in relation to the zygomatic arch; the dorsal edge of the zygomatic arch being located more posterior and dorsal, deepening the arch and extending it behind the orbit; and a narrower frontal plate between the orbits.

PC2 accounted for 11.8% of all variance and the subspecies of *T. stigmatica* were separated along this axis (Fig. 4a). At the negative extreme of PC2, where the majority of *T. s. stigmatica* are located, the nasal apertures and tip of the muzzle are more extended, creating a longer muzzle, and the base and tip of the muzzle are further separated dorso-ventrally, creating a taller muzzle. All landmarks of the zygomatic arch are situated more medially, resulting in a thinner cranium, and the orbit margin is located relatively posteriorly and closer to the cranial midline. The majority of *T. s. stigmatica* are located in this region. At the positive extreme of PC2 lie the majority of *T. s. wilcoxi*. Here, the nasal apertures and tip of the muzzle are closer to the cranium, and the zygomatic arch landmarks

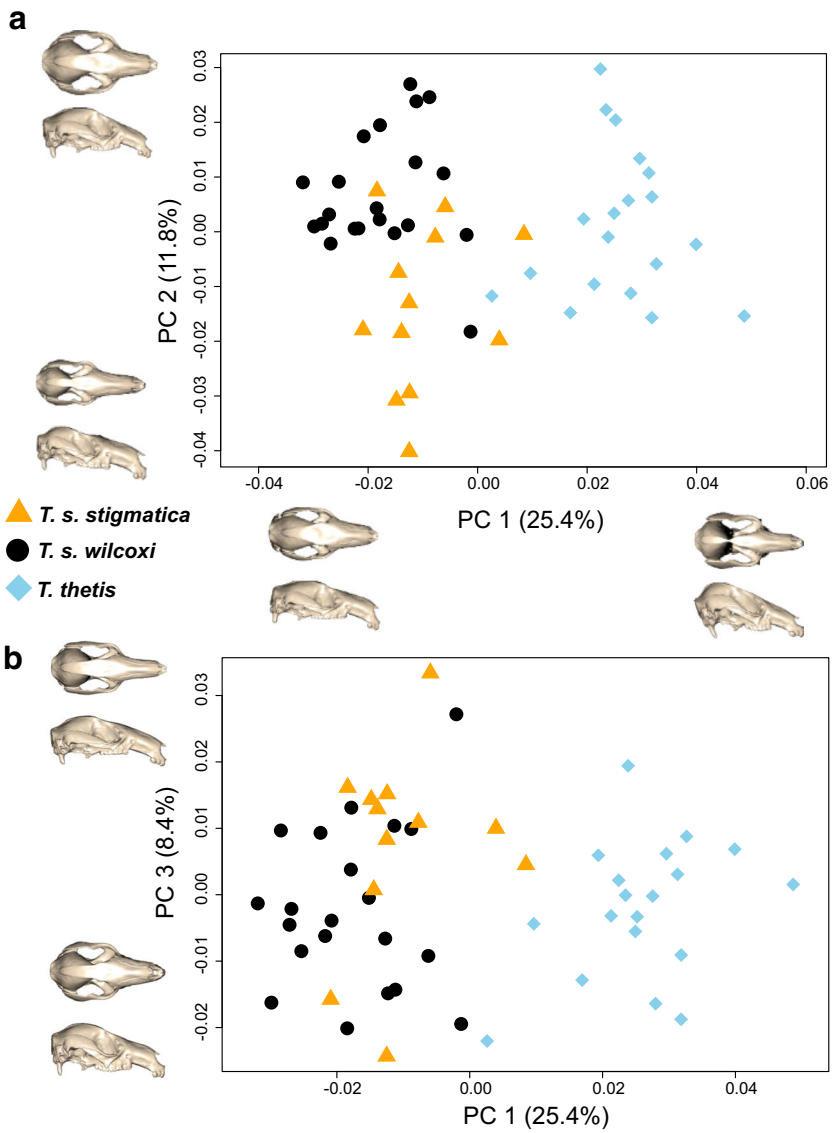

Fig. 4 Principal component analyses of the three *Thylogale* taxa. Warps represent morphological differences along each respective component; magnified ×3 for clarity

are situated more laterally, together creating a shorter, broader cranium. The dorsal margin of the orbit is also shifted more antero laterally here, widening the frontal plate. Despite the two subspecies having some overlap along this axis, a significant difference in cranial morphology was also found between these two taxa alone ($R^2 = 0.12$, $F_{(1,31)} = 4.06$, $P = 0.001$). The distribution of *T. thetis* is broader along this axis, but more skewed towards the positive end, with *T. s. wilcoxi*.

The third principal component contributed 8.4% of the total variation and was associated with the dorsal morphology of the nares and the dorso-ventral positioning of the masseteric process (Fig. 4b). However, all species were evenly spread across this component, with *T. s. stigmatica* representing both extremes. All further components contributed less than 5% of the variation and are not considered further here.

Finite Element Analysis

The perMANOVAs revealed several points along the muzzle and zygomatic arch that differ significantly between species and subspecies during different biting actions (Table 3). Most differences in strain magnitudes were found during the incisor bite. For these loadings, the muzzle, dorsal zygomatic arch, ventral zygomatic arch, and diastema returned significant differences between groups. For the premolar bite, differences were found at the ventral orbit ridge, the ventral zygomatic arch, and the diastema. The molar bite returned significantly different strain magnitudes at the ventral orbit ridge and dorsal zygomatic arch (Table 3).

This represents a novel approach to assessing fine-scale variations in strain distributions of finite element models. However, the small sample size of six individuals per group

Table 3 perMANOVAs for each curve indicated in Fig. 3. Bold indicates significant differences in strain magnitudes ($P < 0.05$), underlined indicates near significance ($P < 0.08$). DR = dorsal muzzle, VOR = ventral orbit ridge, DZA = dorsal zygomatic arch, VZA = ventral zygomatic arch, AMP = anterior masseteric process, D = lateral diastema

Comparison	DR	VOR	DZA	VZA	AMP	D
Incisors (all groups)	**0.001**	0.231	**0.024**	**0.002**	0.329	**0.015**
T. s. stigmatica vs *T. thetis*	**0.007**	0.379	**0.006**	**0.009**	0.089	**0.011**
T. s. stigmatica vs *T. s. wilcoxi*	**0.017**	0.522	0.058	**0.007**	0.814	0.575
T. thetis vs *T. s. wilcoxi*	**0.013**	0.09	0.443	0.174	0.226	**0.022**
Premolar (all groups)	0.122	0.184	0.205	0.15	0.497	0.071
T. s. stigmatica vs *T. thetis*	0.079	0.946	0.168	0.154	0.652	0.48
T. s. stigmatica vs *T. s. wilcoxi*	0.232	**0.031**	0.667	**0.014**	0.627	0.228
T. thetis vs *T. s. wilcoxi*	0.197	0.232	0.075	0.557	0.205	0.05
Molar (all groups)	0.49	**0.003**	**0.033**	0.345	0.492	0.167
T. s. stigmatica vs *T. thetis*	0.167	0.064	0.083	0.74	0.289	0.426
T. s. stigmatica vs *T. s. wilcoxi*	0.545	**0.042**	0.492	0.058	0.881	0.146
T. thetis vs *T. s. wilcoxi*	0.712	**0.019**	**0.017**	0.356	0.296	0.076

suggests a risk of type 1 errors in significance. Regions with only one point of significance should be interpreted with caution, due to such risks. Alternatively, serial instances of curves with standard deviations of strain magnitudes that do not overlap provide a much stronger basis for argument and these are what we have discussed in greater detail. The strain magnitudes of these curves, the dorsal muzzle and ventral zygomatic arch during an incisor bite, are presented with confidence intervals in Fig. 5. Where the confidence intervals do not overlap, there are significant differences in strain at these semilandmarks. Strain magnitudes for all curves under each of the three loadings can be found in the supplementary material (Figs. S5-S7), along with the finite element models displaying strain maps for each simulation (Figs. S8-S10).

During the incisor bite, *T. thetis* exhibits greater strain than both *T. stigmatica* subspecies along most of the length of the muzzle (Fig. 5a). In addition, the distribution of strain shows opposing trends along the muzzle for the subspecies. While *T. s. stigmatica* has higher strain at the muzzle base and lower magnitudes towards the tip, the reverse is found for *T. s. wilcoxi*, which displays significantly higher strain at the muzzle tip than both other groups (Fig. 5a). The zygomatic arch exhibits greater strain in *T. s. stigmatica* than in *T. thetis* and *T.s. wilcoxi* during an incisor bite (Fig. 5b), a trend also observed during a premolar bite (Fig. S6).

Discussion

Among the pademelon taxa examined, we found significant interspecific and intraspecific differences in cranial morphology and performance. The regions of the cranium found to contribute substantially to the among-taxa variation were associated with mechanical efficiency and masticatory muscle attachment sites, including the length and robustness of the muzzle and the morphology of the zygomatic arches. Both geography and climate influenced these shape differences, and the FEMs confirm that these morphologies have a significant impact on biomechanical performance during feeding behaviors. The fine-scale morphological differences found in the muzzle morphology between these pademelon taxa agree with broad-scale differences found across the Macropodiformes (Janis 1990; Mitchell et al. 2018): *T. thetis* frequently possesses a longer muzzle, more often found in grazers; *T. s. wilcoxi* has a broader cranium exhibiting a shorter, more robust muzzle, as for browsing species; and *T. s. stigmatica* possesses a relatively gracile skull with a longer muzzle, as expected for species that focus on less resistant vegetation.

Cranial shape varies with latitudinal gradient and climate in the pademelons studied, which is also the case for several studies across other macropod taxa (Milne and O'Higgins 2002; Hadley et al. 2009; Dawson and Milne 2012). Usually these patterns concern changes to muzzle morphology. It has been suggested that a larger muzzle allows improved efficiency in the warming and humidification of inspired air; and the muzzle has been found to be shorter and broader in warmer climates among potoroids (Johnston and Sharman 1976) and quokkas (*Setonix brachyurus*) (Dawson and Milne 2012). Yet, our results display the opposite trend for the two subspecies of *T. stigmatica*, with the warmer-climate subspecies showing significantly longer, more gracile muzzle morphology. Milne and O'Higgins (2002) found that increasing latitude was associated with increasing muzzle length, but decreasing height across species of *Macropus*. We have similar findings for muzzle height, but not length in *Thylogale*. Muzzle morphology in *T. stigmatica* appears to be less influenced by respiratory efficiency demands or osmoregulation (Hadley et al. 2009) and more by feeding regimes, as muzzle morphology more closely follows biomechanical predictions determined from dietary ecology (Janis 1990; Mitchell et al. 2018).

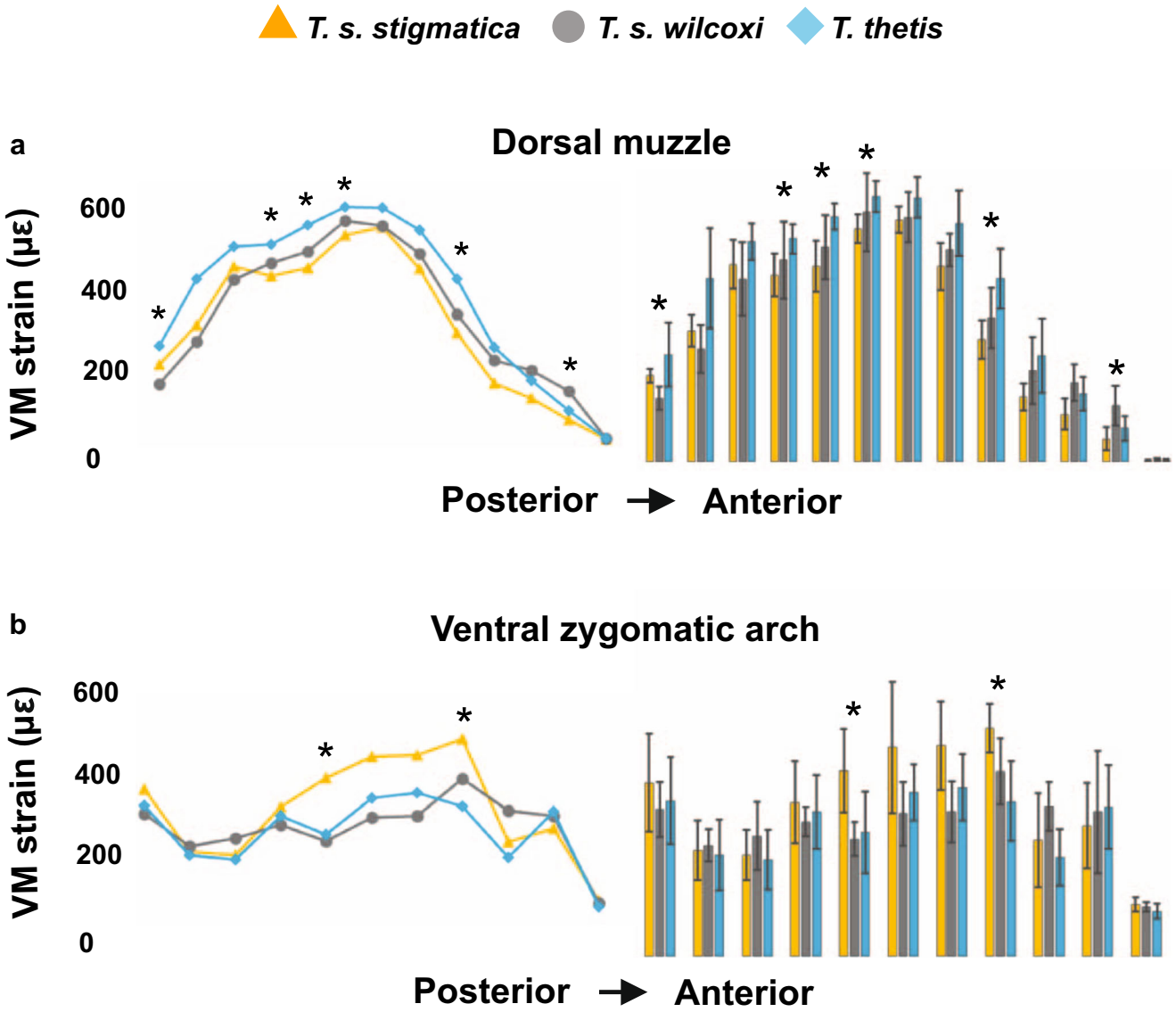

Fig. 5 Strain distributions along (**a**) the dorsal muzzle during an incisor bite and (**b**) the ventral zygomatic arch during an incisor bite. Bars indicate standard deviation and asterisks indicate where significant differences are present

All three taxa showed significant differences in biomechanical performance, particularly in the distribution and magnitude of strain along the muzzle during an incisor bite. The relatively greater strain exhibited along the majority of the muzzle of *T. thetis* is consistent with the more gracile morphology of other grazing herbivores (Janis 1990; Mitchell et al. 2018). Despite the lower strain magnitudes found in both *T. stigmatica* subspecies, the longer muzzle of *T. s. stigmatica* is more similar to *T. thetis* and results in greater deformation at the base of the muzzle. By contrast, the shorter, more robust muzzle found in browsers correlates with greater mechanical efficiency and a relatively stronger bite reaction force closer to the incisors (Therrien 2005; Goswami et al. 2011; Wroe et al. 2010). The results for *T. s. wilcoxi* display significantly less strain at the muzzle base, and greater strain towards the tip of the muzzle. This indicates that *T. s. wilcoxi* has a relatively reinforced muzzle base, resulting in a concentrated bite reaction force at the anterior; better suited to slicing through more resistant vegetation than the other two taxa.

We found evidence of increased temporalis muscle mass in *T. s. wilcoxi*, as observed in other browsing species (Warburton 2009), which would assist with such cropping behaviors. The temporalis is the second largest jaw adductor in macropods (27–37% of adductor muscle mass) and serves to raise and retract the mandible (Warburton 2009). *Thylogale s. wilcoxi* have zygomatic arches that were farther displaced from the braincase. The cross-sectional area of the temporalis muscle is reflected in the size and width of the infratemporal fossa (Thomason 1991). It is likely that the wider zygoma found in this subspecies can accommodate larger temporalis muscles. By contrast, *T. s. stigmatica* displayed a reduced infratemporal fossa, indicating a corresponding reduction in

the temporalis muscle. This suggests that *T. s. stigmatica* do not possess the musculature capable of producing bites as powerful as *T. s. wilcoxi*.

The combination of a long muzzle and reduced zygomatic arch in *T. s. stigmatica* suggests relatively reduced biomechanical constraints for feeding. The muzzle of macropods of similar sizes will likely only increase in relative length if preferred foods are less resistant, or the use of cervical musculature reduces the need for hard biting (Mitchell et al. 2018). The ability to pluck graze by tension frees the cranium of grazers from much of the strain undergone when feeding on browse and biting on harder, more resistant items (Sanson 1989) and the weaker muzzle of *T. thetis* reflects this. *Thylogale s. stigmatica* have a long muzzle that also meets these predictions; however, the weaker performance along the zygomatic arch of this subspecies may be also related to latitudinal differences in vegetation properties. This is suggested by the VARPART analysis via significant differences attributed to geography and climate. In regions with less rainfall and soil nutrients, leaves tend to possess smaller cells with thicker cell walls, thicker lamina, and denser leaf tissue (Turner 1994; Cunningham et al. 1999). The interactions we found with the environmental variables (geography and climate) support the conclusion that *T. s. stigmatica* obtains and processes softer vegetation than *T. s. wilcoxi* (see Jarman and Phillips 1989; Vernes 1995). The strain magnitudes obtained from the zygomatic arch also support the suggestion that *T. s. stigmatica* is less capable of obtaining and processing resistant vegetation, while *T. s. wilcoxi* is more proficient at removing hard browse items from temperate sclerophyllous plants of higher latitudes. The similarly low strain along the zygomatic arch of *T. thetis* suggests that this species is better suited to processing tougher graze from higher latitudes.

Several aspects of cranial shape variation between the two species also correspond with allometric variation across all macropodiforms (Mitchell et al. 2018). Larger macropods consistently display a well-developed zygomatic arch and an enlarged masseteric process across both extant and extinct species (Flannery 1983; Warburton 2009). The masseteric process was significantly longer in the larger *T. thetis*, while it was less well-developed in both subspecies of *T. stigmatica*. A lack of any significant differences in biomechanical performance along this region suggests it is less likely influenced by biomechanical demands and more a product of allometric muscle scaling (Alexander 1985). In addition, a narrower frontal plate is observed in larger species, bringing the orbits closer together towards the midline of the cranium (Mitchell et al. 2018). The narrower frontal plates in *T. thetis* follow this trend. However, a wider distance between temporalis origins also orients the muscle fibers more vertically above the coronoid process, and may assist with more focused vertical jaw movements, as suggested for extinct short-faced sthenurine kangaroos (Prideaux 2004). In addition, wider frontal plates may provide bony buttressing to reinforce the muzzle base, contributing to the low strain magnitudes observed in this region for the browsing *T. s. wilcoxi*.

Macqueen et al. (2010) suggested that *T. stigmatica* recolonized the east coast, during the early Pliocene, after allopatric speciation from *T. thetis*. The contrasting features in cranial morphology of *T. s. wilcoxi* are hypothesized to be a product of niche displacement within the sympatric range, as suggested by Jarman et al. (1987) and Vernes (1995), and subsequent dietary specialization. However, this hypothesis cannot be reasonably established without first comparing specimens that originate from allopatric localities to the north of the range of *T. s. wilcoxi*, for which none were available in Australian collections to study here. The occurrence of some overlap in morphospace between subspecies implies some shared aspects of cranial shape. It is possible that, in an absence of *T. thetis*, *T. s. wilcoxi* could incorporate more graze into its diet, resulting in corresponding craniofacial adaptations. However, the significantly different strain magnitudes suggest there are fundamental differences in the underlying bone structure. Such phenotypic differences may be a product of Haversian remodeling of bone through the lifetime of the animal (Lieberman 1997), brought about by the noted dietary differences between the taxa. Regardless of the underlying mechanisms at this scale, feeding ecology presents an influence on craniofacial morphology among these taxa to a subspecies level. This suggests that dietary dependence is reflected in the crania to this scale in at least some other kangaroos and wallabies, which may be of use in the formulation of conservation and management strategies for vulnerable and endangered species.

Acknowledgements Work was supported by ARC Discovery Grants DP140102659 and DP140102656 to S.W. The authors would like to thank Stuart Green of the University of New England and staff of the UNE Natural History Museum, Sandy Ingleby of the Australian Museum, and Heather Janetzki of the Queensland Museum for allowing access to their respective collections; Karl Vernes for freely sharing his extensive knowledge of pademelons; and Karl Little of Armidale Radiology for CT acquisition and Tzong-Tyng Hung of the BRIL and National imaging facility at UNSW for CT scanning specimens.

References

Adams DC, Collyer M, Kaliontzopoulou A, Sherratt E (2016) Geomorph (Version 3.0.2,): Geometric Morphometric Analyses of 2D/3D Landmark Data

Alexander RM (1985) The maximum forces exerted by animals. J Exp Biol 115: 231–238

Borcard D, Legendre P (2002) All-scale spatial analysis of ecological data by means of principal coordinates of neighbour matrices. Ecol Model 153: 51e68. https://doi.org/10.1016/S0304-3800(01)00501-4

Borcard D, Legendre P, Avois-Jacquet C, Tuomisto H (2004) Dissecting the spatial structure of ecological data at multiple scales. Ecology 85: 1826e1832. https://doi.org/10.1890/03-3111

Carotenuto F, Di Febbraro M, Melchionna M, Castiglione S, Saggese F, Serio C, Mondanaro A, Passaro F, Loy A, Raia P (2016) The

influence of climate on species distribution over time and space during the late Quaternary. Quaternary Sci Rev 149: 188–199. https://doi.org/10.1016/j.quascirev.2016.07.036

Clauss M, Kaiser T, Hummel J (2008) The morphophysiological adaptations of browsing and grazing mammals. In: Gordon IJ, Prins HHT (eds) The Ecology of Browsing and Grazing. Springer, Heidelberg, pp 47–88

Cunningham SA, Summerhayes B, Westoby M (1999) Evolutionary divergences in leaf structure and chemistry, comparing rainfall and soil nutrient gradients. Ecol Monograph 69(4): 569–588. https://doi.org/10.1890/0012-9615(1999)069[0569:EDILSA]2.0.CO;2

Dawson R, Milne N (2012) Cranial size and shape variation in mainland and island populations of the quokka. J Zool 288(4): 267–274. https://doi.org/10.1111/j.1469-7998.2012.00952.x

Eldridge MDB, Heckenberg K, Neaves LE, Metcalfe CJ, Hamilton S, Johnson, PM, Close RL (2011) Genetic differentiation and introgression amongst *Thylogale* (pademelons) taxa in eastern Australia. Aust J Zool 59(2): 103–117. https://doi.org/10.1071/ZO11022

Flannery TF (1983) Revision of the macropodid subfamily Sthenurinae (Marsupialia: Macropodidae) and the relationships of the species of *Troposodea* and *Lagostrophus*. Aust Mammal 6: 15–28

Fortuny J, Marcé-Nogué J, Heiss E, Sanchez M, Gil L, Galobart À (2015) 3D bite modeling and feeding mechanics of the largest living amphibian, the Chinese giant salamander *Andrias davidianus* (Amphibia: Urodela). PLoS One 10(4): e0121885. https://doi.org/10.1371/journal.pone.0121885

Goswami A, Milne N, Wroe S (2011) Biting through constraints: cranial morphology, disparity and convergence across living and fossil carnivorous mammals. Proc R Soc Lond B Biol Sci 278: 1831–1839. https://doi.org/10.1098/rspb.2010.2031

Grosse IR, Dumont ER, Coletta C, Tolleson A (2007) Techniques for modeling muscle-induced forces in finite element models of skeletal structures. Anat Rec 290: 1069–1088. https://doi.org/10.1002/ar.20568

Hadley C, Milne N, Schmitt LH (2009) A three-dimensional geometric morphometric analysis of variation in cranial size and shape in tammar wallaby (*Macropus eugenii*) populations. Aust J Zool 57(5): 337–345. https://doi.org/10.1071/ZO08098

Janis CM (1990) Correlation of cranial and dental variables with dietary preferences in mammals: a comparison of macropodoids and ungulates. Mem Queensland Mus 28(1): 349–366

Jarman PJ (1984) The dietary ecology of macropod marsupials. Proc Nutrition Soc Australia 9(8): 82–87

Jarman PJ, Phillips CM (1989) Diets in a community of macropod species. In: Grigg G, Jarman P, Hume I (eds) Kangaroos, Wallabies and Rat-kangaroos. Surrey Beatty, NSW, Australia, pp 143–149

Jarman PJ, Johnson CN, Southwell CJ, Stuartdick R (1987) Macropod studies at Wallaby Creek. 1. The area and animals. Wildl Res 14(1): 1–14

Johnson KA (1977) Ecology and management of the red-necked pademelon, *Thylogale thetis*, on the Dorrigo plateau of northern New South Wales. PhD thesis, University of New England, Armidale

Johnson KA (1980) Spatial and temporal use of habitat by the red-necked pademelon, *Thylogale thetis* (Marsupialia: Macropodidae). Wildl Res 7(2): 157–166

Johnson PM, Vernes K (2008) Red-legged pademelon *Thylogale stigmatica*. In: van Dyck S, Strahan R (eds) The Mammals of Australia, 3rd edn. New Holland Publishers, Sydney, pp 397–400

Johnston PG, Sharman GB (1976) Studies on populations on *Potorous* Desmarest (Marsupialia) I. Morphological variation. Aust J Zool 24(4): 573–588

Klingenberg CP (2013) Visualizations in geometric morphometrics: how to read and how to make graphs showing shape changes. Hystrix 24: 15–14

Klingenberg CP, Barluenga M, Meyer A (2002) Shape analysis of symmetric structures: quantifying variation among individuals and asymmetry. Evolution 56(10): 1909–1920. https://doi.org/10.1554/0014-3820(2002)056[1909:SAOSSQ]2.0.CO;2

Kupczik K, Dobson CA, Crompton RH, Phillips R, Oxnard CE, Fagan MJ, O'Higgins P (2009) Masticatory loading and bone adaptation in the supraorbital torus of developing macaques. Am J Phys Anthropol 139(2): 193–203. https://doi.org/10.1002/ajpa.20972

Ledogar JA, Dechow PC, Wang Q, Gharpure PH, Gordon AD, Baab KL, Smith AL, Weber GW, Grosse IR, Ross CF, Richmond BG, Wright BW, Byron C, Wroe S, Strait DS (2016) Human feeding biomechanics: performance, variation, and functional constraints. PeerJ 4: e2242. https://doi.org/10.7717/peerj.2242

Legendre P (2008) Studying beta diversity: ecological variation partitioning by multiple regression and canonical analysis. J Plant Ecol 1(1): 3e8. https://doi.org/10.1093/jpe/rtm001

Legendre P, Borcard D, Roberts DW (2012) Variation partitioning involving orthogonal spatial eigenfunction submodels. Ecology 93(5): 1234e1240. https://doi.org/10.1890/11-2028.1

Legendre P, Legendre L (2012) Numerical Ecology, 3rd edn. Elsevier Science BV, Amsterdam.

Lieberman DE (1997) Making behavioral and phylogenetic inferences from hominid fossils: considering the developmental influence of mechanical forces. Annu Rev Anthropol 26(1): 185–210. https://doi.org/10.1146/annurev.anthro.26.1.185

Macqueen P, Seddon JM, Austin JJ, Hamilton S, Goldizen AW (2010) Phylogenetics of the pademelons (Macropodidae: *Thylogale*) and historical biogeography of the Australo-Papuan region. Mol Phylogenet Evol 57(3): 1134–1148. https://doi.org/10.1016/j.ympev.2010.08.010

Macqueen P, Seddon JM, Goldizen AW (2012) Effects of historical forest contraction on the phylogeographic structure of Australo-Papuan populations of the red-legged pademelon (Macropodidae: *Thylogale stigmatica*). Aust Ecol 37(4): 479–490. https://doi.org/10.1111/j.1442-9993.2011.02309.x

Milne N, O'Higgins P (2002) Inter-specific variation in *Macropus* crania: form, function and phylogeny. J Zool 256(4): 523–535. https://doi.org/10.1017/S0952836902000572

Mitchell DR, Sherratt E, Ledogar JA, Wroe S (2018) The biomechanics of foraging determines face length among kangaroos and their relatives. Proc R Soc B 285: 20180845. https://doi.org/10.1098/rspb.2018.0845

Nalla RK, Kinney JH, Ritchie RO (2003) Mechanistic fracture criteria for the failure of human cortical bone. Nat Mater 2: 164–168. https://doi.org/10.1038/nmat832

Oksanen J, Blanchet FG, Kindt R, Legendre P, Minchin PR, O'hara RB, Simpson GL, Solymos P, Stevens MHH, Wagner H (2013) Vegan: Community Ecology Package. R package, version 2.0e10.

Oldfield CC, McHenry CR, Clausen PD, Chamoli U, Parr WCH, Stynder DD, Wroe S (2011) Finite element analysis of ursid cranial mechanics and the prediction of feeding behaviour in the extinct giant *Agriotherium africanum*. J Zool 286(2): 171–171. https://doi.org/10.1111/j.1469-7998.2011.00862.x

Parr WCH, Wroe S, Chamoli U, Richards HS, McCurry MR, Clausen PD, McHenry C (2012) Toward integration of geometric morphometrics and computational biomechanics: new methods for 3D virtual reconstruction and quantitative analysis of Finite Element Models. J Theor Biol 301: 1–14. https://doi.org/10.1016/j.jtbi.2012.01.030

Pierce SE, Angielczyk KD, Rayfield EJ (2008) Patterns of morphospace occupation and mechanical performance in extant crocodilian skulls: a combined geometric morphometric and finite element modeling approach. J Morphol 269(7): 840–864. https://doi.org/10.1002/jmor.10627

Pierce SE, Angielczyk KD, Rayfield EJ (2009) Shape and mechanics in thalattosuchian (Crocodylomorpha) skulls: implications for feeding

behaviour and niche partitioning. J Anat 215(5): 555–576. https://doi.org/10.1111/j.1469-7580.2009.01137.x

Piras P, Marcolini F, Raia P, Curcio M, Kotsakis T (2010) Ecophenotypic variation and phylogenetic inheritance in first lower molar shape of extant Italian populations of *Microtus* (*Terricola*) *savii* (Rodentia). Biol J Linn Soc 99(3): 632–647. https://doi.org/10.1111/j.1095-8312.2009.01379.x

Prideaux GJ (2004) Systematics and evolution of the sthenurine kangaroos. Univ Calif Publi Geol Sci 146: 1–623

R Development Core Team (2016) R: a language and environment for statistical computing. Vienna. URL http://www.R-project.org

Rayfield EJ (2007) Finite element analysis and understanding the biomechanics and evolution of living and fossil organisms. Annu Rev Earth Planet Sci 35: 541–576. https://doi.org/10.1146/annurev.earth.35.031306.140104

Rohlf FJ, Slice D (1990) Extensions of the Procrustes method for the optimal superimposition of landmarks. Syst Zool 39(1): 40–59. https://doi.org/10.2307/2992207

Sansalone G, Bertè DF, Maiorino L, Pandolfi L (2015a) Evolutionary trends and stasis in carnassial teeth of European Pleistocene wolf *Canis lupus* (Mammalia, Canidae). Quaternary Sci Rev 110: 36–48. https://doi.org/10.1016/j.quascirev.2014.12.009

Sansalone G, Kotsakis T, Piras P (2015b*) Talpa fossilis* or *Talpa europaea*? Using geometric morphometrics and allometric trajectories of humeral moles remains from Hungary to answer a taxonomic debate. Palaeontol Electr 18.2.42A. https://doi.org/10.26879/560

Sanson GD (1989) Morphological adaptations of teeth to diets and feeding in the Macropodoidea. In: Grigg G, Jarman P, Hume I (eds) Kangaroos, Wallabies and Rat-kangaroos. Surrey Beatty, NSW, Australia, pp 151–168

Sharp AC (2015) Comparative finite element analysis of the cranial performance of four herbivorous marsupials. J Morphol 276(10): 1230–1243. https://doi.org/10.1002/jmor.20414

Sherratt E, Gower DJ, Klingenberg CP, Wilkinson M (2014) Evolution of cranial shape in caecilians (Amphibia: Gymnophiona). Evol Biol 41(4): 528–545. https://doi.org/10.1007/s11692-014-9287-2

Shipley LA (1999) Grazers and browsers: how digestive morphology affects diet selection. In: Launchbaugh KL, Sanders KD, Mosley JC (eds.) Grazing Behavior of Livestock and Wildlife. University of Idaho, Moscow, pp 20–27

Smith AL, Benazzi S, Ledogar JA, Tamvada K, Pryor Smith LC, Weber GW, Spencer MA, Dechow PC, Grosse IR, Ross CF, Richmond BG, Wright BW, Wang Q, Byron C, Slice DE, Strait DS (2015a) Biomechanical implications of intraspecific shape variation in chimpanzee crania: moving toward an integration of geometric morphometrics and finite element analysis. Anat Rec 298(1): 122–144. https://doi.org/10.1002/ar.23074

Smith AL, Benazzi S, Ledogar JA, Tamvada K, Pryor Smith LC, Weber GW, Spencer MA, Lucas PW, Michael S, Shekeban A, Al-Fadhalah K, Almusallam AS, Dechow PC, Grosse IR, Ross CF, Madden RH, Richmond BG, Wright BW, Wang Q, Byron C, Slice DE, Wood S, Dzialo C, Berthaume MA, van Casteren A, Strait DS (2015b) The feeding biomechanics and dietary ecology of *Paranthropus boisei*. Anat Rec 298(1): 145–167. https://doi.org/10.1002/ar.23073

Strait DS, Grosse IR, Dechow PC, Smith AL, Wang Q, Weber GW, Neubauer S, Slice DE, Chalk J, Richmond BG, Lucas PW, Spencer MA, Schrein C, Wright BW, Byron C, Ross CF (2010) The structural rigidity of the cranium of *Australopithecus africanus*: implications for diet, dietary adaptations, and the allometry of feeding biomechanics. Anat Rec 293: 583–593. https://doi.org/10.1002/ar.21122

Therrien F (2005) Feeding behaviour and bite force of sabretoothed predators. Zool J Linn Soc 145(3): 393–426. https://doi.org/10.1111/j.1096-3642.2005.00194.x

Thomason JJ (1991) Cranial strength in relation to estimated biting forces in some mammals. Can J Zool 69(9): 2326–2333

Turner IM (1994) Sclerophylly: primarily protective? Funct Ecol 8(6): 669–675

Vernes K (1995) The diet of the red-legged pademelon *Thylogale stigmatica* (Gould) (Marsupialia: Macropodidae) in fragmented tropical rainforest, north Queensland, Australia. Mammalia 59(4): 517–526

Wahungu GM, Catterall CP, Olsen MF (1999) Selective herbivory by red-necked pademelon *Thylogale thetis* at rainforest margins: factors affecting predation rates. Aust J Ecol 24(6): 577–586. https://doi.org/10.1046/j.1442-9993.1999.01005.x

Warburton NM (2009) Comparative jaw muscle anatomy in kangaroos, wallabies, and rat-kangaroos (Marsupialia: Macropodoidea). Anat Rec 292(6): 875–884. https://doi.org/10.1002/ar.20905

Wroe S, Ferrara TL, McHenry CR, Curnoe D, Chamoli U (2010) The craniomandibular mechanics of being human. Proc R Soc Lond B Biol Sci 277: 3579–3586.

Zelditch ML, Swiderski DL, Sheets HD, Fink WL (2004) Geometric Morphometrics for Biologists: A Primer. Elsevier, San Diego